Plume Dynamics of the 2021 La Soufrière Eruption

Geri Peykova

March 27, 2024

Abstract

The 2021 eruption of La Soufrière volcano on the island of St Vincent consisted of a series of eruptive events occurring over 14 days. This project focuses on understanding the dynamics of the ash plumes of the different events during this period and determining the ascent rates by accurately estimating plume heights. A novel method based on the observation of buoyancy waves within the plume was developed. This method uses high temporal resolution satellite imagery from the Advanced Baseline Imager (ABI) to track the evolution of the volcanic plume during each event. By analyzing the formation of buoyancy waves and the ambient conditions, the plume heights during multiple events were estimated and compared to heights obtained through other methods. The insights gained from this analysis contribute to our understanding of volcanic eruption dynamics and hazard management.

1 Introduction

La Soufrière is a stratovolcano (elevation 1220m), located on the island of St. Vincent in the Caribbean at 13.33°N latitude and 61.18°W longitude. It is part of the Eastern Caribbean volcanic arc. La Soufrière has exhibited explosive and effusive eruptions. It has a long history of volcanic activity dating back centuries, with recorded explosive eruptions occurring in 1718, 1812, 1902, and 1979. The most recent eruption took place in April 2021 after 42 years of dormancy. This event produced pyroclastic flows, lava flows, and extensive ashfall, covering the island in a thick layer of ash and causing widespread disruption.

Increased seismic activity was recorded in late 2020 and was followed by an effusive eruption that formed a new lava dome. On April 9, 2021, a series of explosive eruptions began and lasted for 14 days. The start time and duration of the different events can be inferred from the seismic data, (summarized in Sparks et al., 2021). Taylor et al. (2023) offers a detailed chronology of the eruption obtained through satellite observations. The eruption consisted of multiple events divided into four phases: (1) initial explosive event, (2) sustained ash emission, (3) pulsatory phase (25 events between 10-12 April), (4) waning phase (8 events between 13-22 April). In the paper, the heights of the plumes are also estimated by comparing the observed brightness temperature (BT) as measured in the 11.2 μm band with a theoretical BT calculated based on atmospheric conditions (later referred as the BT method). Most of the plumes reached a height of $15 - 19$ km placing them near the tropopause. The temperature inversion at the tropopause however means that there are often two possible solutions, one stratospheric and one troposheric. Horvath et al. (2022) used a geometric approach to estimate the heights. The GOES-West satellite offers a side angle (zenith angle of 85°) view of the volcano allowing for direct measurement using the visual bands during the day and infrared bands at night. The IR however has a significantly lower resolution and this method produces accurate estimates only when daylight observations are possible.

Mathematical models like Baines (2013) explain how volcanic plumes spread in a density-stratified atmosphere, considering both static atmospheres and strong unidirectional winds. Internal waves that arise within the plumes are also discussed. In-depth observations of these waves have not been made before as high-frequency data have only recently become available.

Understanding plume dynamics is significant for aviation, climate, and hazard management. This report aims to explore the plume dynamics of the 2021 eruption of La Soufrière and compute important parameters such as height and ascent rate.

2 Methods

2.1 Instruments

2.1.1 The Advanced Baseline Imager

For this study, we used data from the Advanced Baseline Imager (ABI), installed on the Geostationary Operational Environmental Satellite East (GOES-East or GOES-16). The satellite was launched in 2016 and it's positioned at 75.2° W. The coverage area of GOES-16 spans North, Central and South America, the Caribbean, the Eastern Pacific, and the North Atlantic Ocean. The ABI instrument consists of 16 channels between 0.45-13.7 μm, with spatial resolutions 0.5 km for visible bands and 2 km for infrared bands at nadir. The 8.4 μm and 11.2 μm bands provide sensitivity for ash detection. During the La Soufrière eruption, GOES-16's ABI captured a new full-disc image every 10 minutes. Additionally, GOES-16 offers two movable mesoscale regions, each covering an area of 1000×1000 km, allowing for data updates every minute. These regions are repositioned to provide more frequent observations during events like severe weather and wildfires. During the La Soufrière eruption, one of the mesoscale regions was directed over the volcano, between 9:00 UTC on April 10, 2021 and 06:00 UTC on April 16, 2021, providing increased temporal coverage of the volcanic activity during the pulsatory phase and the first four events of the waning phase.

2.1.2 ERA5

ERA5 was used for the tempreture and pressure profiles in this study. ERA5 (ECMWF Reanalysis 5) is a global atmospheric reanalysis dataset produced by the European Centre for Medium-Range Weather Forecasts (ECMWF). It combines observational data from various sources, such as weather stations, satellites, and buoys, with a numerical weather model to produce a gridded representation of the Earth's climate system. It covers the entire globe on a 30 km grid and provides data at various altitudes from the surface up to 80 km. Data is available at hourly time intervals. The parameters used in this study include temperature, pressure and the u and v vector components of the wind velocity. The four nearest profiles were interpolated to the volcano's location to produce the profiles used in this study.

2.2 Buoyancy wave model

Buoyancy waves are generated when parcels of air (in this case containing ash) are vertically displaced from the level of neutral buoyancy (LNB) and the buoyancy tries to restore equilibrium. The parcels oscillate about LNB at the Brunt-Vaisala frequency N which depends on the ambient conditions:

$$N^2 = \frac{g}{\theta}\frac{d\theta}{dz}.$$

In the expression above g is the acceleration due to gravity, z is the altitude and θ is the potential temperature defined as:

$$\theta = T\frac{P_0}{P}^{R/c_p},$$

where T is the current temperature of the parcel, P is the pressure, P_0 is a reference pressure, R is the gas constant and c_p is the specific heat capacity at constant pressure. For air, $R/c_p = 0.286$. Combining the two equations and assuming hydrostatic equilibrium, $\frac{dP}{dz} = -\rho g$, and ideal gas, $\rho = \frac{PM}{RT}$, where ρ is the density and $M = 29$ g/mol is the molar mass, we get the Brunt-Vaisala frequency in terms of temperature, pressure and some constants:

$$N^2 = \frac{g^2 M}{RT}(\frac{R}{c_p} - \frac{d\ln T}{d\ln P}). \tag{1}$$

This expression allows us to reconstruct hourly oscillation frequency profiles using ERA5 data.

Periodic variations in temperature in the plume in the 8.4 μm and 11.2 μm bands (ABI channels 11 and 14 respectively), interpreted as waves in the umbrella region, were observed in most of the events during the increased temporal coverage period. The frequencies of these oscillations were mapped to the heights of the umbrella regions based on frequency profiles of the atmosphere calculated from ERA5 data.

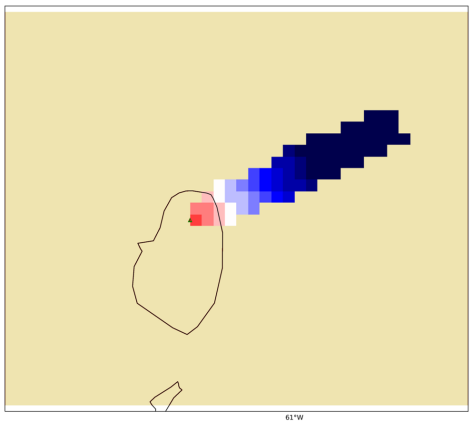

Figure 1: Pixel selection: map of the island of St Vincent (green triangle indicates the location of La Soufrière) with a rectangular transect at 60°. Red shells are closer to the vent and dark blue shells are further away.

2.2.1 Data extraction and filtering

Temperature data was obtained from the 11.2 μm band, which is sensitive to ash and captures the movement of the plume downwind and the cylindrical wavefronts of the buoyancy waves within it. Concentric rings of pixels, each of width 1 grid cell (roughly 2 km), were constructed around the vent. Within these rings, pixels in a rectangular transect aligned with the wind direction for each specific event were used to compute the average temperature for each ring (Figure 1). The average temperature of the shells was then tracked as it changed with time (Figure 2).

The temporal and spatial temperature data were cropped to the region of interest where waves could be easily discerned. For event 11, this involved selecting data points with distances greater than 5 grid units and times between 20 and 50 minutes. Subsequently, a high-pass filter was applied to eliminate the background noise. A Butterworth 4^{th}-order filter with a cutoff frequency ranging from 0.2 to 0.4 was used, and the optimal cutoff frequency was determined to be 0.33 for event 11 (Figure 3).

2.2.2 Parameter fitting

The data was fitted with a simple plane wave equation of the form:

$$T(x,t) = A\cos\left(kx - \omega t - \phi\right) \tag{2}$$

In this equation, A is the amplitude, k is the wavenumber or the spatial frequency,x is the distance from the vent, ω is the frequency (equivalent to the Brunt-Vaisala frequency, N), t is the time and ϕ represents the phase angle. For simplicity, the impact of wind on the frequency N was ignored (discussed in section 2.2.5). Additionally, damping coefficients (both temporal and spatial) or the cylindrical nature of the waves were not considered.

The Brunt-Vaisala frequency was determined through fitting for events 6, 11, 19 and 20 from the pulsatory phase and event 28 from the waning phase (Figure 3, Table 1).

2.2.3 Height estimation

The Brunt-Vaisala frequency profiles were calculated using Eq. 1. These profiles were derived from temperature and pressure data averaged over the period from 1-8 April, obtained from ERA5 data during the closest hour of the day. The fitted frequencies were compared to the atmosphere profiles to get the height of the umbrella region, as illustrated in Figure 4. The frequencies and the corresponding heights are summarized in Table 1. This method yielded a single solution for all of the events that were considered.

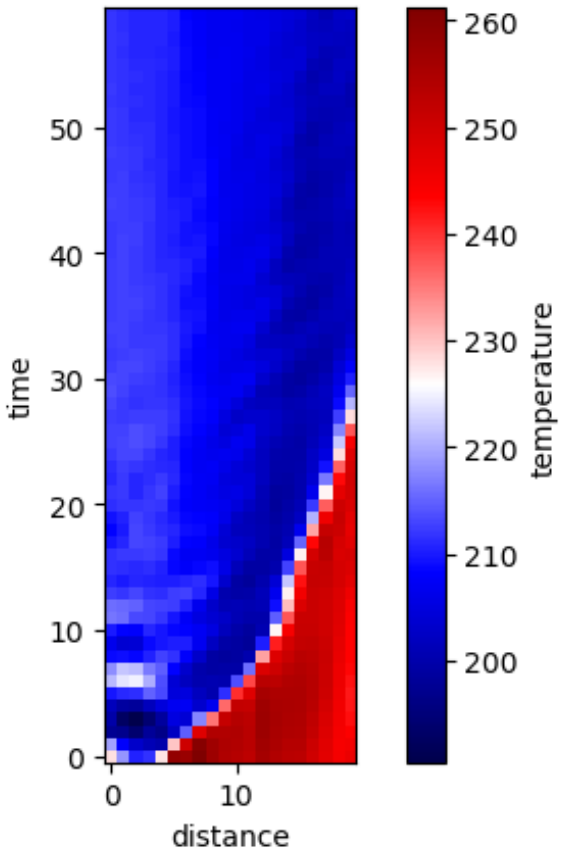

Figure 2: Plume temperature of event 11 from the 11.2 μm channel as a function of time (in minutes) and distance of shells from the vent (in grid coordinates). The buoyancy waves can be clearly seen in the upper half part of the plot. The lower right corner is red as the the ash plume hasn't spread this far immediately after the eruption. The dark blue spot in the lower left corner suggests the formation of an overshooting top.

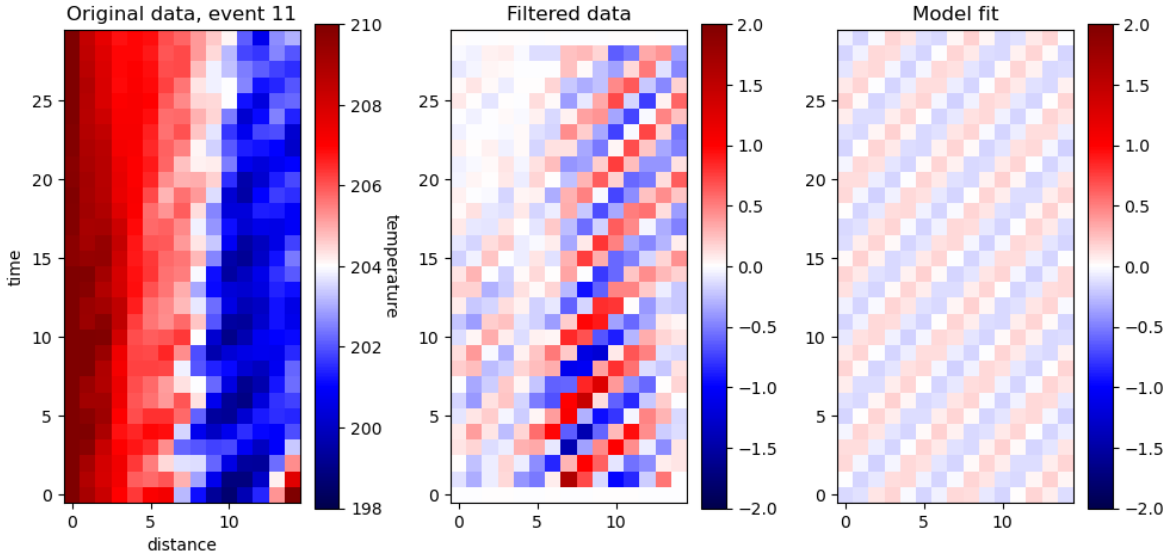

Figure 3: Plume temperature of event 11 from the 11.2 μm channel as a function of time (in minutes) and distance of shells from the vent (in grid coordinates): (a) original data cropped to the region of interest; (b) data after a high-pass filter with cutoff frequency 0.33 was applied; (c) best model fit.

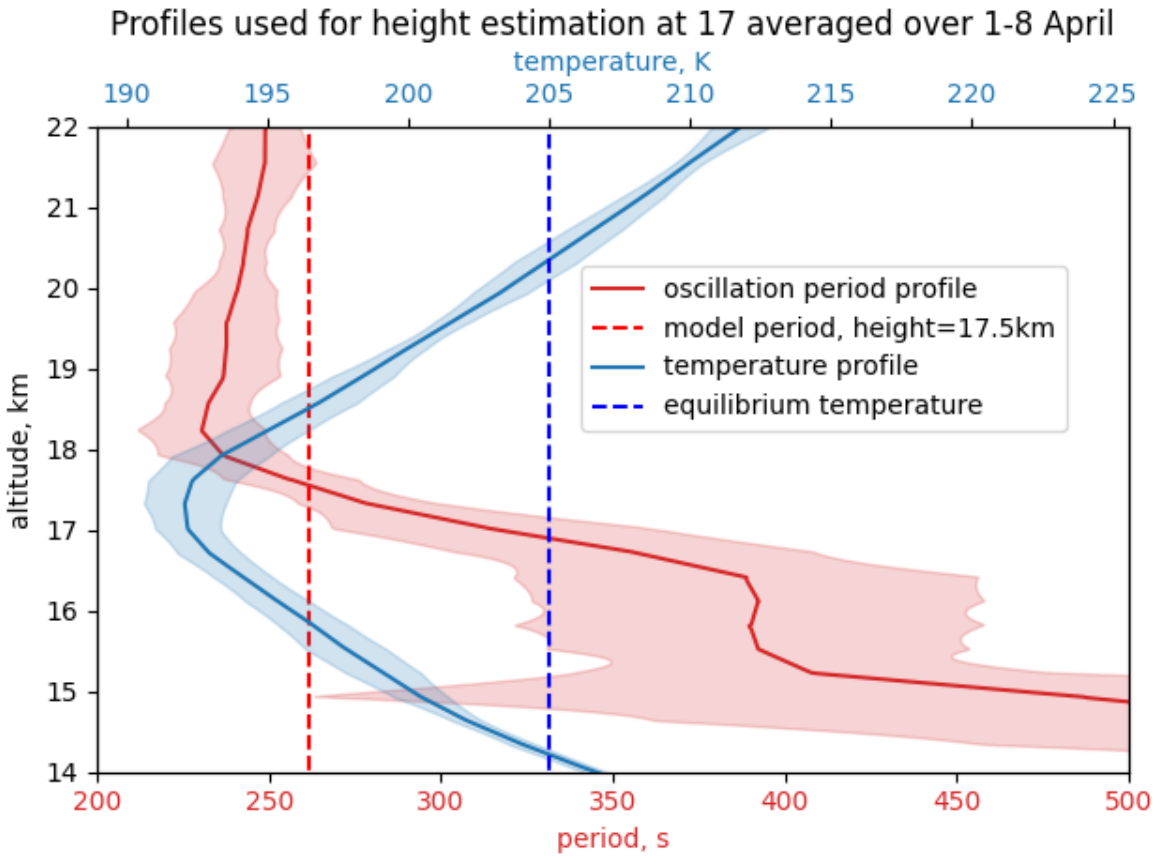

Figure 4: The solid lines are the averaged oscillation period and temperature profiles at 17:00 over the 1-8 April period derived from ERA5 data. Shaded regions represent the standard deviation. The dashed lines are the fitted/measured parameters for event 11. The red lines intersect once, meaning that there is one solution (17.5 km) using the buoyancy wave method. The BT method (in blue) produces two solutions: one in the troposphere (14.2 km) and one in the stratosphere (20.3 km).

event	Brunt-Vaisala frequency, min^{-1}	plume height, km	ascent time, min	ascent rate, m/s
6	1.36 ± 0.01	17.6±0.1	12	23±4
11	1.44 ± 0.006	17.5±0.1	6	45±15
19	1.1 ± 0.03	16.8±0.1	11	24±4
20	1.21 ± 0.02	17±0.1	9	29±7
28	0.97 ± 0.03	15.9± 0.45	17	14±2

Table 1: Fitted and calculated parameters for some of the eruptive events.

2.2.4 Ascent rates

The ascent rates, v_{ascent}, were computed using the formula

$$v_{ascent} = \frac{z_{\text{plume}} - z_{\text{volcano}}}{t_{\text{umbrella}} - t_{\text{start}}}, \tag{3}$$

where z_{plume} is the height of the umbrella, $z_{\text{volcano}} = 1220$ m is the elevation of the volcano, t_{start} is the start time of the eruption and t_{umbrella} is the time when the ash plume reached the umbrella height. Start times were determined from the seismic data as reported in Sparks et al. (2023). The beginning of an event is defined as the onset of the seismic signal associated with that particular event. To determine t_{umbrella}, the equilibrium temperature T_0 were first calculated by averaging the temperatures of the shells of pixels located at distances greater than 5 grid units. The time when a pixel within a box surrounding the vent reached this equilibrium temperature was recorded as t_{umbrella}. The error in the difference in timings was set to 2 minutes for all events.

2.2.5 Static atmosphere assumption

While ignoring the wind is an oversimplification, it is not entirely unjustified. If the phase velocity, $v_p = \omega/k$, is much greater than the wind speed, v_w, the effect of the latter is negligible. Plugging in the parameters fitted with plane wave model, we get that $v_p \approx 60$m/s which is about a magnitude larger than the wind speed at the plume altitude derived from ERA5, $v_w \approx 5$ m/s. However, future models should incorporate wind effects to yield more accurate results. The presence of cross-wind means that the fitted frequency is lower than the actual frequency, implying that the height estimates should be regarded as upper boundaries.

2.3 Adiabatic rise model

Overshooting tops (OTs) were observed in most of the events from the increased temporal coverage period. Notably, all events that produced waves also had an overshooting top. This model attempts to understand the dynamics of the OTs.

The adiabatic rise model assumes that the ash plume reaches an altitude at which its temperature T_0 matches the atmospheric temperature. This is the umbrella height. From there, the parcel rises adiabatically until it reaches a minimum temperature T_{min}. At this stage, the parcel is colder than the surrounding air so it becomes unstable and collapses. The pressure of the parcel at its coldest point is calculated by plugging in the initial temperature T_0 and pressure and the final temperature T_{min} into the adiabatic condition:

$$P^{1-\gamma}T^{\gamma} = constant$$

where P is the pressure of the parcel, T is temperature, $\gamma = c_p/c_v$ and c_p and c_v are the specific heat capacities at constant pressure and volume respectively. The final pressure is then matched to a height which represents the OT height.

The minimum temperature T_{min} is determined by finding the minimum temperature reached in a box around the vent within 20 minutes of the start of the eruption. The equilibrium temperature T_0 is computed by taking the average temperature over the plume. This is translated to an altitude and subsequently pressure using the BT method with the 11.2 μm channel. As the plumes from this eruption end up somewhere around the tropopause, this method gives rise to two solutions for the umbrella height and two possible adiabats for the OT, one stratospheric and one troposheric (Figure 5). The stratospheric solution results are recorded in Table 2.

	stratospheric solution	
event	umbrella, km	OT, km
6	19.8	20.9
11	21.1	23.3
19	19.8	20.5
20	19.9	20.7
28	19.8	20.3

Table 2: Stratospheric solutions for the plume heights of some of the eruptive events calculated using the adiabatic rise model.

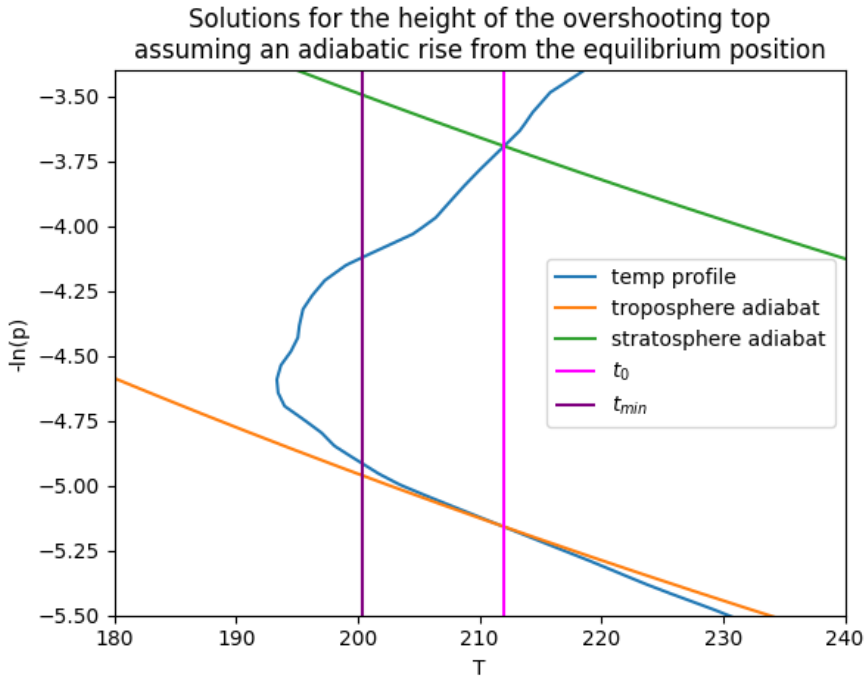

Figure 5: Adiabatic rise model. The intersection points of t_0 (pink) and the temperature profile (blue) indicate the umbrella height estimates. The green and orange curves are the strotospheric and tropospheric adiabats respectively. The heights of the OTs can determined from the pressure of the intersection points of the adiabats and $t_{\min}$ (purple).

3 Results

3.1 Bouyancy wave model

The computed plume heights were compared with those measured by Horvath et al. (2022) using the side angle technique (see Figure 6). All plumes reach a height of 16-19 km, placing them at or slightly above the tropopause. In general, the geometric estimates tend to be higher as the side angle method measures the top of the umbrella region. In contrast, the buoyancy wave model calculates the level of neutral buoyancy, which is positioned lower within the umbrella region. The difference between the heights obtained from these two methods could potentially be used to estimate the thickness of the umbrella region. Nevertheless, the buoyancy wave estimates follow the same trend as the side angle estimates which demonstrates the viability of the new method. Interestingly, the heights calculated using the 8.4 μm and 11.2 μm bands were nearly identical. This suggests that the plume oscillates at a single frequency, making this method less sensitive to the optical thickness of the plume and the channel used for detection.

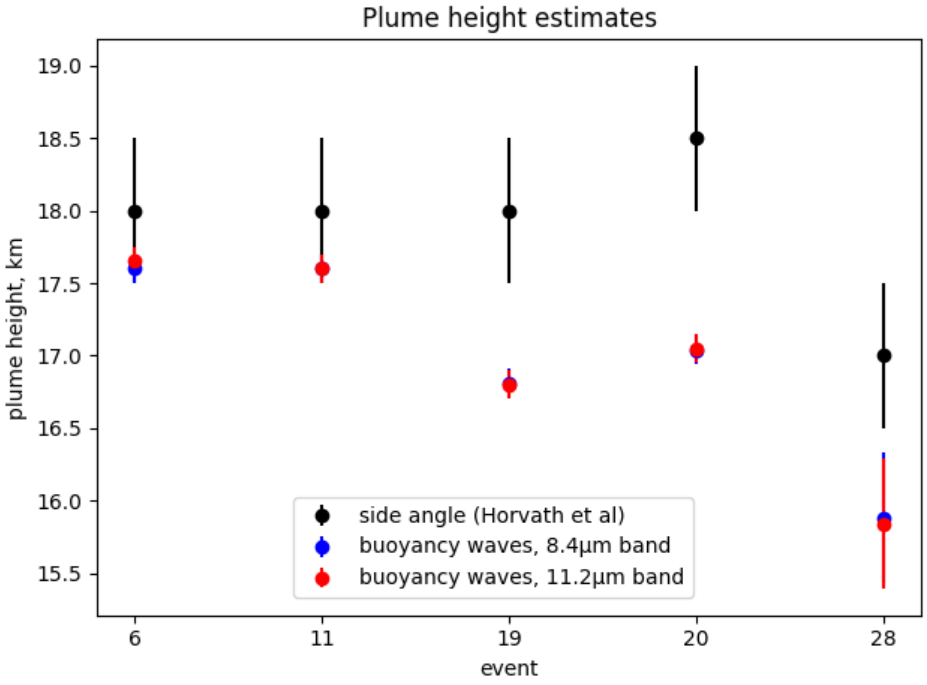

Figure 6: Comparison of plume height estimates using the side angle view and buoyancy waves methods. The geometric estimates are bigger as they represent the top of the umbrella region while the buoyancy wave method measures the level of neutral buoyancy which is situated at a lower altitude. The difference between the two could be used to approximate the thickness of the umbrella. The heights calculated using the 8.4 μm and 11.2 μm bands are nearly identical.

3.2 Adiabatic rise model

The stratospheric solutions for umbrella and OT heights were also compared to the side angle view estimates from Horvath et al. (Figure 7). This method was less successful. When matching the plume equilibrium temperature to the ambient temperature, the umbrella heights obtained placed the plume higher in the atmosphere. Additionally, the computed heights of the OTs did not correspond to the side view estimates.

Notably, the size of the OTs, which is the difference between the OT and umbrella heights, tended to be significantly smaller when using the adiabatic rise model (approximately 1 km) compared to the side angle estimates (3-4 km). Results became even less consistent when the side angle umbrella height was used as the equilibrium height in the adiabatic rise model. For events 20 and 28, the height of the OT was smaller than the umbrella height, suggesting that the parcel descended instead of ascending, which is not physically plausible.

Overall, the adiabatic rise model did not describe well the dynamics of the formation of OTs.

4 Conclusion

High-frequency satellite data offers new insights into plume dynamics.

A novel method for estimating the height of volcanic eruption plumes by analyzing the waves within them was developed. The advantages of this method include that it provides a single solution for plumes near the tropopause and it is not limited to daylight observations. The method was applied to a range of events from the 2021 La Soufrière eruption and the results closely matched estimates obtained from the side angle view method. This difference between the two estimates could be used to approximate the thickness of the plume. Accurate height estimates allowed ascent rates to be calculated as well. Further testing of this method is necessary, both for events from the La Soufrière eruption and, when data is available, in other volcanic eruptions. Future research should focus on refining the method by improving pixel sampling, considering additional parameters such as damping

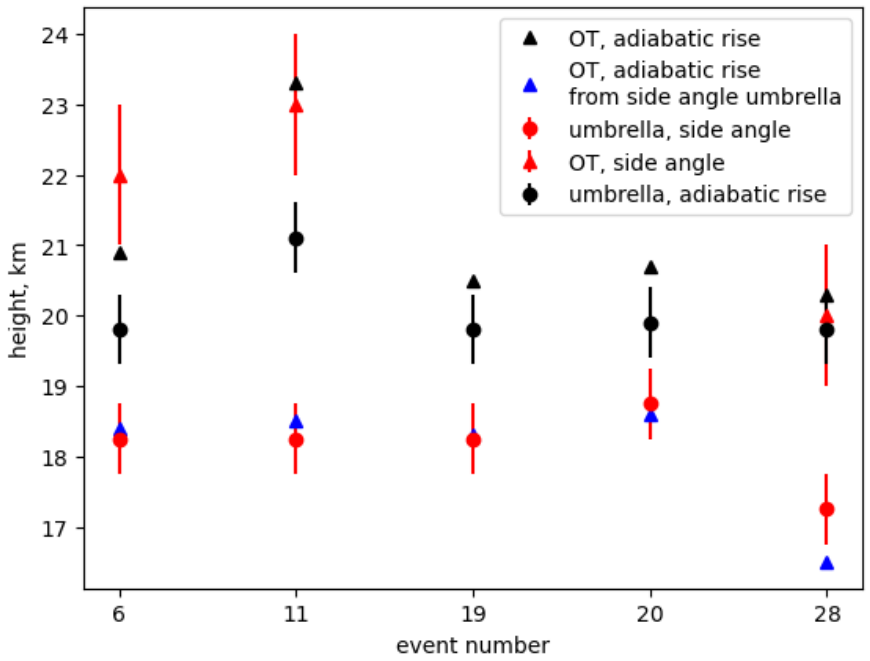

Figure 7: Comparing umbrella and OT height estimates from the side angle view method (Horvath et al. (2022) in red) and the stratospheric solutions from the adiabatic rise model (in black). Blue triangles indicate the OT height assuming that the parcel rises adiabatically from the umbrella height reported by Horvath et al. (2022)

coefficients, and incorporating wind into the model. Spatial damping coefficients can reveal how energy propagates within the volcanic plume. Investigating whether oscillations decay over time can provide insights into their origin, whether they are continuously generated or triggered by specific events, such as the collapse of the overshooting top.

The proposed adiabatic rise model considerably underestimated the size of the overshooting tops (OTs). Therefore, it is evident that OTs are not formed by a simple adiabatic ascent of parcels of ash from the umbrella height. To provide a more accurate description of the dynamics governing their formation, alternative models should be explored and improved criteria for identifying parcel instability that leads to collapse should be established.

References

[1] Baines, P.G. 2013: The dynamics of intrusions into a density-stratified crossflow. *Physics of Fluids* 25, 076601, 1-30.

[2] Horváth, Á., Carr, J. L., Wu, D. L., Bruckert, J., Hoshyaripour, G. A., and Buehler, S. A.: Measurement report: Plume heights of the April 2021 La Soufrière eruptions from GOES-17 side views and GOES-16–MODIS stereo views, *Atmos. Chem. Phys.*, 22, 12311–12330, https://doi.org/10.5194/acp-22-12311-2022, 2022.

[3] Sparks, S., Aspinall, W., Barclay, J., Renfrew, I., C.-A. R., and Stewart, R.: Analysis of magma flux and eruption intensity during the 2021 explosive activity at the Soufrière of St Vincent, West Indies, *Geological Society, London, Special Publications*, 539, in press.

[4] Taylor, I. A., Grainger, R. G., Prata, A. T., Proud, S. R., Mather, T. A., and Pyle, D. M.: Satellite measurements of plumes from the 2021 eruption of La Soufrière, St Vincent, *Atmos. Chem. Phys.* Discuss. [preprint], https://doi.org/10.5194/acp-2022-772, in review, 2022.